Author(s): Khuyagbaatar, J.; Yakushev, A.; Düllmann, Ch. E.; Ackermann, D.; Andersson, L.-L.; Asai, M.; Block, M.; Boll, R. A.; Brand, H.; Cox, D. M.; Dasgupta, M.; Derkx, X.; Nitto, A. Di; Eberhardt, K.; Even, J.; Evers, M.; Fahlander, C.; Forsberg, U.; Gates, J. M.; Gharibyan, N.; Golubev, P.; Gregorich, K. E.; Hamilton, J. H.; Hartmann, W.; Herzberg, R.-D.; Heßberger, F. P.; Hinde, D. J.; Hoffmann, J.; Hollinger, R.; Hübner,

Title: Fusion reaction 48Ca+249Bk leading to formation of the element Ts (Z=117)

Year: 2019

Version: Published version

Fusion reaction ^{48}Ca+^{249}Bk leading to formation of the element Ts ($Z = 117$)

J. Khuyagbaatar,[1,2,*] A. Yakushev,[2] Ch. E. Düllmann,[1,2,3] D. Ackermann,[2,†] L.-L. Andersson,[1] M. Asai,[4] M. Block,[2] R. A. Boll,[5] H. Brand,[2] D. M. Cox,[6,‡] M. Dasgupta,[7] X. Derkx,[1,3] A. Di Nitto,[3] K. Eberhardt,[1,3] J. Even,[1,§] M. Evers,[7] C. Fahlander,[8] U. Forsberg,[8] J. M. Gates,[9] N. Gharibyan,[10] P. Golubev,[8] K. E. Gregorich,[9] J. H. Hamilton,[11] W. Hartmann,[2] R.-D. Herzberg,[6] F. P. Heßberger,[1,2] D. J. Hinde,[7] J. Hoffmann,[2] R. Hollinger,[2] A. Hübner,[2] E. Jäger,[2] B. Kindler,[2] J. V. Kratz,[3] J. Krier,[2] N. Kurz,[2] M. Laatiaoui,[2] S. Lahiri,[12] R. Lang,[2] B. Lommel,[2] M. Maiti,[12,‖] K. Miernik,[5] S. Minami,[2] A. Mistry,[6,¶] C. Mokry,[1,3] H. Nitsche,[9,**] J. P. Omtvedt,[13] G. K. Pang,[9] P. Papadakis,[6,14] D. Renisch,[3] J. Roberto,[5] D. Rudolph,[8] J. Runke,[2] K. P. Rykaczewski,[5] L. G. Sarmiento,[8] M. Schädel,[2,4] B. Schausten,[2] A. Semchenkov,[13] D. A. Shaughnessy,[10] P. Steinegger,[15,16] J. Steiner,[2] E. E. Tereshatov,[10,††] P. Thörle-Pospiech,[1,3] K. Tinschert,[2] T. Torres De Heidenreich,[2] N. Trautmann,[3] A. Türler,[15,16] J. Uusitalo,[14] D. E. Ward,[8] M. Wegrzecki,[17] N. Wiehl,[1,3] S. M. Van Cleve,[5] and V. Yakusheva[1]

[1]*Helmholtz Institute Mainz, 55099 Mainz, Germany*
[2]*GSI Helmholtzzentrum für Schwerionenforschung, 64291 Darmstadt, Germany*
[3]*Johannes Gutenberg-Universität Mainz, 55099 Mainz, Germany*
[4]*Advanced Science Research Center, Japan Atomic Energy Agency, Tokai, Ibaraki 319-1195, Japan*
[5]*Oak Ridge National Laboratory, Oak Ridge, Tennessee 37831, USA*
[6]*University of Liverpool, Liverpool L69 7ZE, United Kingdom*
[7]*The Australian National University, Canberra, ACT 0200, Australia*
[8]*Lund University, 22100 Lund, Sweden*
[9]*Lawrence Berkeley National Laboratory, Berkeley, California 94720, USA*
[10]*Lawrence Livermore National Laboratory, Livermore, California 94551, USA*
[11]*Vanderbilt University, Nashville, Tennessee 37235, USA*
[12]*Saha Institute of Nuclear Physics, Kolkata 700064, India*
[13]*University of Oslo, 0315 Oslo, Norway*
[14]*University of Jyväskylä, 40351 Jyväskylä, Finland*
[15]*Paul Scherrer Institute, 5232 Villigen, Switzerland*
[16]*University of Bern, 3012 Bern, Switzerland*
[17]*The Institute of Electron Technology, 02-668 Warsaw, Poland*

(Received 18 February 2019; published 7 May 2019)

The heaviest currently known nuclei, which have up to 118 protons, have been produced in ^{48}Ca induced reactions with actinide targets. Among them, the element tennessine (Ts), which has 117 protons, has been synthesized by fusing ^{48}Ca with the radioactive target ^{249}Bk, which has a half-life of 327 d. The experiment was performed at the gas-filled recoil separator TASCA. Two long and two short α decay chains were observed. The long chains were attributed to the decay of ^{294}Ts. The possible origin of the short-decay chains is discussed in comparison with the known experimental data. They are found to fit with the decay chain patterns attributed to ^{293}Ts. The present experimental results confirm the previous findings at the Dubna Gas-Filled Recoil Separator on the decay chains originating from the nuclei assigned to Ts.

DOI: 10.1103/PhysRevC.99.054306

I. INTRODUCTION

During the past two decades the experimental attempts to reaching the island of stability, i.e., nuclei at around the predicted $Z = 114$ and $N = 184$, have had great successes resulting in the discoveries of elements with atomic numbers up to $Z = 118$ [1–3]. The heaviest nuclei ($Z > 111$) associated with island of stability have been observed in complete fusion reactions of the doubly magic ^{48}Ca ($Z = 20$) used as a projectile and radioactive actinide targets from uranium ($Z = 92$) to californium ($Z = 98$). Such reactions had already been considered for the synthesis of superheavy elements decades ago [4]. However, the sensitivity of those early experiments was not high enough for the observation of superheavy nuclei (SHN) produced as evaporation residues

*J.Khuyagbaatar@gsi.de
†Present address: GANIL, CEA/DSM-CNRS/IN2P3, Bd Henri Becquerel, BP 55027, F-14076 Caen Cedex 5, France.
‡Present address: Lund University, 22100 Lund, Sweden.
§Present address: KVI-Center for Advanced Radiation Technology University of Groningen, 9747 AA Groningen, The Netherlands.
‖Present address: Indian Institute of Technology Roorkee, Roorkee 247667, India.
¶Present address: GSI Helmholtzzentrum für Schwerionenforschung, 64291 Darmstadt, Germany.
**Deceased.
††Present address: Cyclotron Institute, Texas A&M University, College Station, TX 77843, USA.

(ERs) of fusion-evaporation reactions. Overall sensitivities for performing such experiments had significantly been improved at the Dubna Gas-Filled Recoil Separator (DGFRS) at the Flerov Laboratory of Nuclear Reactions in Dubna, Russia. As a result it became possible to produce SHN closer to the island of stability in ^{48}Ca induced fusion reactions [2]. To date, several results from the DGFRS on the elements Cn (Z = 112), Fl (Z = 114), Mc (Z = 115), Lv (Z = 116), and Ts (Z = 117) have been confirmed across a number of laboratories by using the same ^{48}Ca + actinide fusion-evaporation reactions [5–15]. Confirmation experiments aimed at studying chemical properties of Cn, Nh (Z = 113), and Fl (see review article [16]) were carried out as well.

The success of the ^{48}Ca-induced reactions were reasonably high evaporation residue cross sections (order of pb for the range of Z = 112–118) observed for almost all cases. These are often attributed to gains in fusion probabilities, and effects of the compound nuclei that are located in the vicinity of the predicted island of stability [2,17,18].

Detailed investigations of these SHN are now one of the main topics in the field. SHN with odd numbers of nucleons are of particular interest as they give access to information on the single-particle states which would help theory to improve the calculations on the structure of the SHN. However, present spectroscopic data, collected exclusively from α decay, are scarce. Only recently, more detailed information on the structure of SHN formed in the decay of Mc [11,13,19] has been obtained by adding γ spectroscopy. However, performing such an experiment for heavier SHN is limited due to lower cross sections. Accordingly, in the heaviest nuclei, α decays still remain the main source for extracting nuclear structure information.

The odd-Z SHN, Mc [2,11,13,19], and Ts [20–23] have been observed with α-decay chains that are relatively long compared to the even-Z ones. Thus, α decay of each member represents valuable information on the structures of various nuclei within wide ranges of Z and N. In this regard, in a recent analysis of all observed α-decay chains assigned to Mc, the possible presence of electron-capture (EC) decay branches in SHN has been inferred [13]. Therefore, a reliable assignment of decay chains originating from the heaviest odd-Z nuclei, which might contain important information on the structure of SHN is often challenging. Ideally, they will be investigated in more detail with advanced experimental techniques, in addition to improved statistics. Recently, an experiment on the direct mass-number measurements of isotopes produced in the fusion-evaporation ^{48}Ca+^{243}Am reaction has successfully been performed and confirmed the mass numbers of ^{288}Mc and ^{284}Nh [15].

Furthermore, the observed relatively long half-lives of the odd-Z SHN allow dedicated experiments to study their electronic shell configurations, which are of great interest in both atomic physics and chemistry.

The element Ts has been synthesized at the gas-filled recoil separator TASCA by using the fusion-evaporation reaction ^{48}Ca+^{249}Bk. The results on the observation of two long decay chains assigned to ^{294}Ts have been published in [12]. Here, we present the experiment in detail together with results of yet unpublished short decay chains.

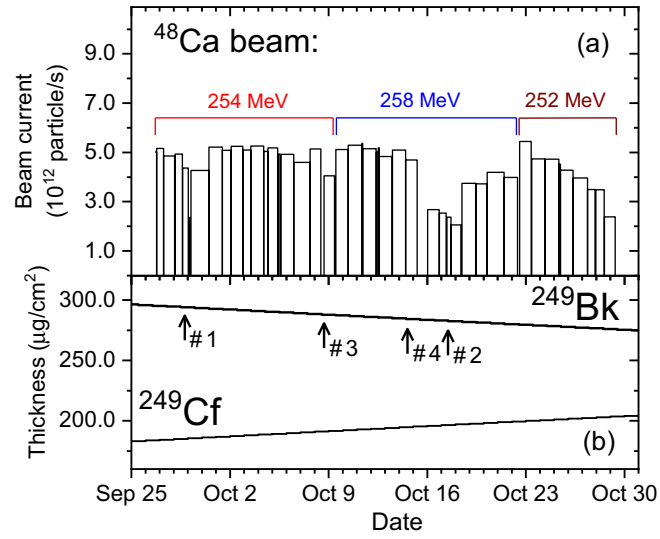

FIG. 1. (a) Average beam currents for each run (254 MeV, 258 MeV, and 252 MeV). (b) Evolution of isotopic thicknesses of ^{249}Bk and ^{249}Cf with average total thickness of 0.48(5) mg/cm^2 during the irradiations by ^{48}Ca beam with energies $E_{\rm lab}$ = 254.0, 258.0, and 252.1 MeV. Arrows indicate the dates when the long (#1 and #2) and short (#3 and #4) chains were detected.

II. EXPERIMENTAL SETUP

A ^{48}Ca^{+10} heavy ion beam was delivered from a 14 GHz electron-cyclotron-resonance (ECR) ion source and was accelerated by the UNIversal LInear ACcelerator (UNILAC) in a pulsed mode with 5 ms pulse-length and 50 Hz repetition frequency. Three different beam energies of 268.3, 270.2, and 274.1 MeV were used. During the whole experiment 1.10×10^{19} ^{48}Ca nuclei irradiated the target within ≈27 d, corresponding to an average beam intensity of 0.75 particle μA (4.7×10^{12} particle per second). In Fig. 1(a), the chronology of beam intensity and energy is shown.

Isotopically pure ^{249}Bk target material was produced at the Oak Ridge National Laboratory (ORNL), USA [24] and a part was then sent to Johanes Gutenberg University Mainz, Germany for the production of the targets. Four target segments with thicknesses of 0.37(4), 0.53(5), 0.53(5), 0.50(5) mg/cm^2 were produced by electrodeposition on 0.99(5) mg/cm^2 Ti-backing foils with an area of 6 cm^2 each [25]. Because the half-life of ^{249}Bk is only 327.2(3) d [26], its amount in the target was continuously decreasing with time via β^- decay to ^{249}Cf (y, [27]), which primarily decays via α particle emission. Initially these targets were first used for an attempt at the synthesis of the element 119 for about four months [28]. The present experiment started about five months later after the target production. The evolution of the average thicknesses of ^{249}Bk and ^{249}Cf in the target is shown in Fig. 1(b). One can see that the amount of ^{249}Bk was already reduced and the target with average total areal density of ≈0.48(5) mg/cm^2 consisted of ^{249}Bk (62%) and its decay product ^{249}Cf (38%) at the beginning of the experiment. The four target segments were mounted on a wheel, which rotates synchronously to the beam pulse structure.

For safety reasons, the target segments were continuously monitored using different methods during the experiment. Their temperature (which proved to be a good quantity for monitoring the target stability during the bombardment) was measured on-line by using a pyrometer [29]. At typical beam intensity of about 0.75 particle μA, a temperature of $\approx$100 °C was recorded by the pyrometer. Alpha particles from the decay of ^{249}Cf accumulating inside the original Bk target were frequently guided to the focal plane detector of TASCA in order to verify target integrity. More detailed descriptions for the handling of the targets are given in Ref. [30].

Before impinging on the target, the beam passed through a 50 μg/cm^2-thick carbon foil mounted on a wheel on the same axis as the target wheel, with both rotating synchronously. The carbon foil was used to increase the initial charge state of incoming ^{48}Ca^{10+} ions to safely deflect them in the TASCA dipole field also in case of accidental appearance of pinholes in the target. Beam energies in the center of the target were estimated by using the SRIM code [31]. Energy losses of ^{48}Ca in the carbon and titanium foils were directly calculated using the data basis of SRIM. For the case of energy loss in the target, its compositions were assumed to have predominantly ^{249}Bk$_2$ ^{16}O$_3$ and/or ^{249}Cf$_2$ ^{16}O$_3$ forms. The three initial beam energies were calculated to result in $E_{\rm lab}$ = 252.1, 254.0, and 258.0 MeV in the center of the target in laboratory frame. Beam energies entering and leaving the target are about $E_{\rm lab}$ + 2.1 MeV and $E_{\rm lab}$ − 2.1 MeV, respectively. Excitation energies of the compound nucleus, ^{297}Ts, formed in complete fusion reactions were estimated by using the known experimental mass excesses of ^{48}Ca, ^{249}Bk [32] and theoretical values for the compound nucleus. Two different mass excess calculations within the Thomas-Fermi [33] and the finite range droplet [34] models were compared. Similar reaction Q values of 171.8 and 170.7 MeV have been predicted by these models. Excitation energies of E^* = 39.5, 41.2, and 44.5 MeV were attributed to ^{297}Ts taking into account that calculations from Ref. [33] are widely used for describing the measured excitation functions of ^{48}Ca + actinide reactions.

Since the gas-filled recoil separator TASCA has been set into operation for superheavy element research in 2008 [35], several experimental campaigns aimed at studying physical and chemical properties of Fl have successfully been carried out in the period 2009–2010 [7,9,36]. TASCA was then significantly upgraded within the framework of the new experimental program aiming at synthesis of elements beyond Og using ^{50}Ti beams [28].

TASCA has the capability to use various gases and also their mixtures for equilibration of the heavy-ion charge states [37]. In the present experiment, TASCA was filled with helium gas at 0.8 mbar pressure. The magnetic settings of the separator were set to guide heavy ions with a magnetic rigidity of $B\rho$ = 2.20 Tm to the center of the focal plane detector. This magnetic rigidity ensures the isolation of ^{293,294}Ts ions with a predicted average charge state of $\approx$7 [38,39]. An efficiency of TASCA for the collection of ERs from the ^{48}Ca+^{249}Bk reaction was estimated by performing Monte Carlo simulations [38]. The highest transmission of 47% was calculated as the best case, e.g., the experimental conditions are correctly accounted for in the simulations.

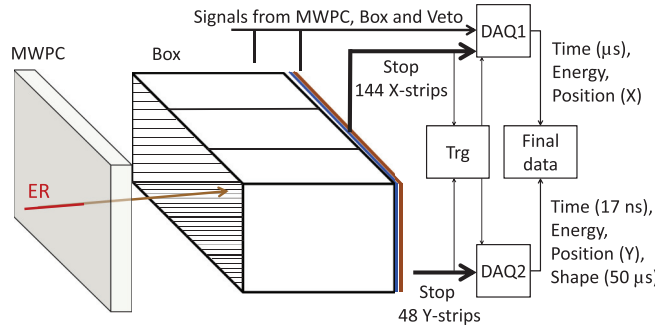

FIG. 2. Schematic illustrations of the focal plane detection setup of TASCA and the Combined ANalog and DIgital (CANDI) data acquisition system coupled to the DSSD stop, box, veto, and MWPC detectors. Data acquisition (DAQ1 and DAQ2) was triggered (Trg) by both X and Y strip signals in 'OR' logical mode. For details, see text.

The ERs passing through TASCA enter the detector chamber and first pass through a multiwire proportional counter (MWPC) filled with isobutane gas (see Fig. 2). The MWPC has two entrance Mylar windows with a thickness of $\approx$2 μm each which separate the helium and isobutane gases at 0.8 and 3 mbar pressures inside TASCA and MWPC, respectively. The MWPC was located $\approx$20 cm upstream of the stop detector. Direct signals from the anode wires (without delay lines), which are proportional to the energy loss of particles passing through, were stored in the data in coincidence (about 5 μs) to any events registered in the implantation detector. Stored MWPC signals were later used for the tagging of events coming through TASCA, to distinguish them from those originating from the decay of implanted nuclei.

The focal plane detection system (FPDS) of TASCA consisted of a double-sided silicon strip detector (DSSD)-based implantation detector (hereafter: stop detector), with eight DSSDs mounted perpendicular in the backward hemisphere of the stop detector to form a five-sided box configuration (hereafter: box detectors). The stop detector comprised 144 vertical (x) and 48 horizontal (y) 1 mm strips on the front and back sides, respectively. The 144 vertical strips faced TASCA and have 0.1 mm strip-pitch. The 48 horizontal strips provide the position information along the y axis. Two adjacent single-sided Si-strip detectors having the same sizes as the stop detector were mounted directly behind the stop detector to register particles passing through the stop detector (veto detector). The veto detector was used to discriminate real α events from low energy signals originating from light particles which passed through the separator and the stop detector [9]. Each box detector had 16 strips on both sides with 72 and 48 mm sizes and longer strips were faced inside the box configuration. In the data processing signals from every two neighboring strips of box detectors were combined. Detailed descriptions of the FPDS are given in Refs. [40,41].

The combined ANalog and DIgital (CANDI) data acquisition system was used for processing the data collected with the FPDS. Signals from the front 144 vertical strips of the DSSD, box, veto, and MWPC detectors were processed in a standard

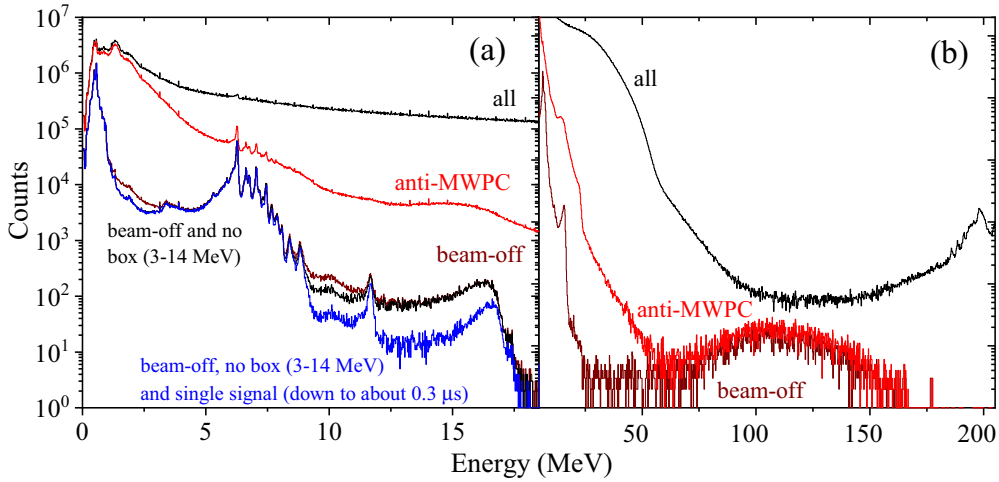

FIG. 3. Low (a) and (b) high energies spectra measured during the 270 MeV run. All, anti-MWPC, and beam-off events are shown. In (a) the spectrum of beam-off events detected solely with the stop detector or no coincidence box detector signal within energies of 3–14 MeV is shown. The spectrum of these events with the additional requirement of having only single-signal traces (digital part of CANDI) is also shown. The algorithm for testing a presence of multisignal traces has a time limit down to 0.3 μs in between signals.

way, i.e., preamplified, amplified and shaped, and digitized by using peak-sensing ADCs. All preamplified signals, except for those from the stop detector's 48 horizontal strips were then further processed via spectroscopic amplifiers with two gains differing by a factor of 11 were used to get two branches for energies of α particles and for high-energetic particles. These signals were independently stored in the analog part of the CANDI, which had a dead-time of $\approx$35 μs (marked as DAQ1 in Fig. 2). Preamplified signals from the horizontal strips of the stop detector were digitized by 60 MHz-sampling ADCs by storing their shapes in 50 μs-long traces (8 μs before and 42 μs after the trigger), marked as DAQ2 in Fig. 2. Finally, both analog and digital DAQs connected to the FPDS were combined as single data events, which allowed the determination of the time, spatial coordinates, beam-on/off status, energy, and shape of each detected event [42]. Advantages of CANDI for the solution of various physics and measurement technical issues have been demonstrated in Refs. [12,37,43–46].

The efficiency for the detection of α particles with full energies in the FPDS is estimated to be 76(4)%. The efficiency for the detection of fission events is 100%. Energy resolutions (FWHM) of individual strips of stop and box detectors were $\approx$40 keV for 5.8 MeV α particles from an external α source placed in front. The final energy calibrations were done using the α decays of nuclei produced in a preparatory ^{50}Ti+^{176}Yb reaction, and of nuclei which are additionally implanted in the stop detector during the experiment as products of reactions not leading to fusion (hereafter; nonfusion products/reactions [47]). In the case of the Y strips of the DSSD, the full energy of an event was not always collected by a single strip but was sometimes shared between neighboring ones while the energy from the front side was collected by a single X strip. An average percentage of such a split signals was 16% throughout all Y strips. The data acquisition was triggered by any event registering more than about 600 keV in a front (X) and/or more than about 500 keV in a back (Y) strips of the stop detector.

Calibration of the high-energy branch was done with an external four α-line source [5]. With such a calibration, the measured energies of fission fragments from ^{256}Rf were distributed in the range of 50–200 MeV [45].

In the present experiment, the highest counting rates for X strips of the stop detector were registered to the "left" side of the detector where mostly the low magnetic rigidity heavy ions originating from nonfusion reactions are detected. The total trigger rate of the FPDS was $\approx$700 Hz at $\approx$0.75 beam current on the target. Half of the counting rate originated from strips $X = 0$ to $X = 34$ and strongly decreased with increasing strip number.

III. EXPERIMENTAL RESULTS AND DISCUSSION

A. Energy spectra and event types

The energy spectra of events measured in the low and high-energy branches (analog part of the data) from the stop detector are shown in Fig. 3. All events registered in all strips of the stop detector resulted in a total counting rate of $\approx$700 Hz. In the anti-MWPC spectrum, i.e., consisting of events detected without a coincident signal from the MWPC, the number of events was significantly reduced. In the analysis, these anti-MWPC signals were considered to be events which might originate from α particles (hereafter, α-like events).

The background of α-like events can be significantly suppressed further by considering only events registered during the 15 ms beam-off period between the UNILAC pulses of 5 ms duration. The spectrum requiring such beam-off α-like events is also shown in Fig. 3(a). This spectrum appears much cleaner and peaks corresponding to α decays are clearly visible [cf. Fig. 3(a)]. A relatively wide peak with a long tail appears at around 16.5 MeV. It is due to pile-up α events, i.e., the summing of energies of α particles detected within a short

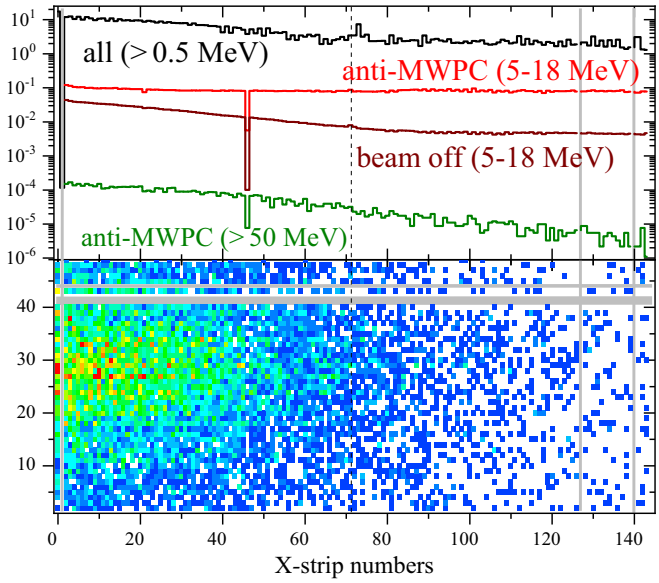

FIG. 4. Upper panel: Horizontal (X strips) distributions of all, anti-MWPC and beam-off low energy events, and fissions measured during the 254 MeV run are shown. Energy windows for selected type of events are given in brackets. Lower panel: X-Y map of spatial distribution of fission events detected during the entire experiment.

time window ($\lesssim 5\,\mu$s). These pile-up events can partially be identified by coincident signals in the box detectors if one of the α particles escaped from the stop detector.

In Fig. 3(a), the spectrum of events detected solely in the stop detector, and with no coincident box-signals with energies of 3–14 MeV, shows a slight decrease of rate in the range of ≈9–12 MeV where the decays of SHN are expected. The region above 12 MeV is not significantly affected because either no escape α particle was detected, the escape energy is < 3 MeV, or both α particles were measured in the stop detector. At the same time, the rate of events within 0.8–3.5 MeV where typical α escape energy releases in the stop detector are recorded, was reduced. Further analyses of pile-up events were done by using their digital traces stored in the second branch of the electronics (DAQ2).

An algorithm enabling a search for multisignal traces was applied for all events, and the spectrum of events containing a single signal in their traces is also shown in Fig. 3(a). While pile-up events were significantly reduced, lines corresponding to α-decay energies remained unchanged. The remaining pile-up events are due to limitations of the algorithm for resolving multiple signals occurring within a very short time ($\lesssim 0.3\,\mu$s). An individual trace containing multiple signals detected within a time between subsequent events down to ≈0.1 μs can be resolved only by visual inspection. Since many α-like events associated with the decay of nuclei originating from nonfusion reactions were detected, we first performed the isotopic identification of α-like events prior to the main analysis searching for the chains of Ts. The results are given in Sec. A 1.

Distributions of various types of events along the X strips of the stop detector are shown in Fig. 4. Beam-off α-like events are accumulated mostly in the left side of the stop detector and indicate the implantation of nuclei with magnetic rigidities lower than the set value. 57% of them were detected in strips $X < 34$. All events measured in the low-energy branch with $E_{\rm stop} > 0.5$ MeV have a distribution similar to that of beam-off α-like events, while anti-MWPC events (5–18 MeV) are equally distributed over all X strips. The behavior of the latter events can be explained by a contribution of low-ionizing particles, e.g., helium, etc., which generate too small charges in the volume of the MWPC to be measured.

The high-energy spectrum of all events contains the recoils originating from the nonfusion reactions, scattered beam, and fission fragments originating from implanted nuclei [see Fig. 3(b)]. The energy spectrum becomes cleaner with the applied anti-MWPC condition. This is due to the efficiency of the MWPC, which is higher for detection of the heavy particles compared to low-energetic light particles. With the beam-off condition, the spectrum is almost free of background, and only events corresponding to fissions and α decays are left. Therefore, anti-MWPC events with energies above 50 MeV were considered to be fission events. In fact, all decay chains originating from the SHN produced in the ^{48}Ca + actinide reactions terminate in fission. Thus, every single fission event was investigated in detail to search for its possible genetic parent (see Sec. A 1). The spatial distribution of fission events is shown in Fig. 4. Several X and Y strips were missing which somewhat reduces the total pixel numbers, but no events were lost, thanks to the combined triggering of CANDI, except for those occurring in the pixels at intersections of nonworking strips.

B. Search for α-decay chains

In the present data analysis by taking into account various possible scenarios for the expected decay chains, first we searched for genetically correlated decay chains in different position and time correlation analyses between implantation (ER), α, and fission (SF) like events. Those candidates found from the correlation analyses were further investigated in more detailed event-by-event analysis, e.g., inspection of the shape (trace) of the signal for each member.

The most promising candidates for such detailed event-by-event analysis were first selected from results of correlation analyses searching for ER–α_1–α_2 ($\Delta t_{ER-\alpha_1} < 1$ s, $\Delta t_{\alpha_1-\alpha_2} < 20$ s) and ER–α_1–α_2–SF ($\Delta t_{ER-\alpha_1} < 20$ s, $\Delta t_{\alpha_1-\alpha_2} < 200$ s, $\Delta t_{\alpha_2-SF} < 500$ s). The search conditions for the first and second α-like events were 8.5–12.0 MeV, and 8–11 MeV, respectively. The energy ranges are strongly overlapping and the searching times are long, thus the random correlation rate will be relatively high, especially for those α-like events detected during beam-on periods. However, these search conditions ensure that also all nonrandom decay chains with 'missing' member(s), e.g., α particles escaping into the backward open hemisphere of the FPDS, will be found.

Energies of ERs originating from the present fusion-evaporation reactions were estimated on the basis of the measured implantation energies of the evaporation residues from the calibration runs with the ^{50}Ti+^{176}Yb and ^{50}Ti+^{206,208}Pb reactions. By assuming a linear dependence between the measured energies of ^{221,222}U and $^{254–256}$Rf and their mass

TABLE I. Average stop detector counting rates of ER-like, α-like, and fission events per pixel are given within the selected energy ranges. Rates of random correlations of various sequences per pixel calculated using the average counting rates and according to Ref. [48] are also given. For the expected average numbers of the random events (N_m), one has to take into account the beam structure to compare with experimental data. Correlation search times (in seconds) are given in brackets.

Event		Counting rate (1/s)	
Type	Energy (MeV)	Beam-on	Beam-off
ER	3–20	1.3×10^{-1}	-
α_1	8.5–12.0	1.0×10^{-3}	1.0×10^{-5}
α_2	8–11	1.2×10^{-3}	1.5×10^{-5}
α_3	8–10	1.0×10^{-3}	1.3×10^{-5}
SF	>50	1.2×10^{-6}	1.0×10^{-6}
Correlation sequences		N_m	
ER–α_1(1)–α_2(20)		2.5	3.1×10^{-4}
ER–α_1(1)–α_2(20)–α_3(300)		1.9×10^{-2}	3.1×10^{-8}
α_1–α_2(20)–α_3(300)		13	2.9×10^{-4}
ER–α_1(20)–α_2(200)–SF(500)		1.8×10^{-4}	2.0×10^{-8}

numbers, an average measured implantation energy of 8 MeV was estimated for mass numbers 293 and 294. Accordingly, any event with energies of 3–20 MeV and coincident to an MWPC signal was considered to be an ER-like event.

Average counting rates of ER-like, α-like, and SF events per pixel of the stop detector during the beam-on and beam-off periods are given in Table I. Expected numbers of random chains corresponding to the different correlation sequences are also given.

In total more than 1000 correlation chains were found for the ER–α_1–α_2 sequence. The majority contained two beam-on α-like events. About 60 chains having the ER–α_1–α_2–SF sequence were found and again most of them contain beam-on α-like events.

Also, α_1–α_2–α_3 correlation searches (see Table I) were applied to ensure the safe identification of chains in case the ER-like signals are outside of the selected range. We found about 2000 chains with triple α-like events in correlation where most of them (92%) were detected with three beam-on α-like events, as expected (cf. Table I).

Finally, as a result of detailed analyses for the presence of various types of correlation sequences, event-by-event, and digital trace inspections, four chains were identified as being nonrandom correlation sequences that do not contain any α particles originating from the decays of nonfusion products. All other chains were attributed to be of random origin and details of such an assignment are given in Sec. A 2, where the analyses of the experimental data are comprehensively described. These four chains were further investigated in more detail and all their members were found and are shown in Table II. Detailed descriptions on the identification of each chain are given in the following sections.

C. Long decay chains

Two chains #1 and #2 containing several α-decaying members were detected at beam energies $E_{\rm lab}$ = 254.0 MeV and 258.0 MeV, respectively. In the initial correlation analysis, α_3, α_7, and fission events of both chains (see Table II) did not appear. These members of the chains were identified in the event-by-event analysis of the corresponding pixels.

TABLE II. Four decay chains identified as nonrandom. Energies and correlation times relative to preceding members are given. The bold font values indicate beam-off events. Energy errors include detector resolutions and calibration uncertainties. The measured fission fragment energies are from stop+box detectors. Details are given in the text.

Chain #	1	2	3	4
Strips (X/Y)	103/41	111/19	47/25,26	12/27,28
E_{ER}	6.8	9.0	6.9	5.3
E_{α_1} (MeV)	**11.07(4)**	**11.02(4)**	**9.70(8)**	**9.87(8)**
$\Delta t_{ER-\alpha1}$	55.9 ms	92.6 ms	8.65 ms	0.49 s
E_{α_2} (MeV)	**10.31(4)**	**10.2(2)**[a]	**10.0(3)**[a]	**9.31(8)**
$\Delta t_{\alpha1-\alpha2}$	2.98 s	0.66 s	76.98 ms	2.57 s
E_{α_3} (MeV)	**9.3(3)**[a]	**4.64**	2.74	–
$\Delta t_{\alpha2-\alpha3}$, (s)	5.96	2.35	0.97	–
E_{α_4} (MeV)	**8.86(3)**	**9.05(3)**	9.34(8)	–
$\Delta t_{\alpha3-\alpha4}$, (s)	172	373	1.44	–
E_{α_5} (MeV)	**9.42(3)**	9.47(3)	–	–
$\Delta t_{\alpha4-\alpha5}$, (s)	6.79	3.53	–	–
E_{α_6} (MeV)	8.84(3)	8.8(2)	–	–
$\Delta t_{\alpha5-\alpha6}$, (s)	45.1	41.3	–	–
E_{α_7} (MeV)	**7.89(3)**	**7.90(3)**	–	–
$\Delta t_{\alpha6-\alpha7}$, (h)	1.3	1.6	–	–
E_{SF} (MeV)	135+7[a]	**189**	89+49[a]	**54**
$\Delta t_{\alpha-SF}$	3.8 h	29 h	0.144 ms	8.42 ms

[a]Total energy of event with coincident stop and box signals.

All α- and fission-like events, which occurred in the pixels X/Y = 103/41 and 111/19, where chains #1 and #2 were found, respectively, are shown in Fig. 5 with their energies ($E_{\rm stop}$) as a function of experimental time. Only one fission event was registered during the entire beam time in each of these pixels. They were detected at about 5 and 31 h after the implantation signals (ER) of chains #1 and #2, respectively. Accordingly, these fission events were attributed to terminate these decay chains.

In the case of chain #1, 55 beam-off α-like events were detected within the energy range of $E_{\rm stop}$ = 7–12 MeV. 32 of them were found to originate from known isotopes, produced in nonfusion reactions (see Sec. A 1). In the energy range of $E_{\rm stop}$ = 8–12 MeV, eight events could not be identified through the correlation analysis as originating from nonfusion products. Four of them occurred within a short time window and were assigned as members of chain #1 (see Table II).

The energies of the remaining four events (8.52, 8.23, 8.86, and 8.89 MeV) are in the range of typical background events where uncorrelated high-energetic α particles commonly appear during experiments on the synthesis of SHN [20]. Such events originate from α decays of ^{212}Po and ^{213}Po, which are populated in the β^- decays of long-lived ^{212}Bi ($T_{1/2}$ = 60.55(6) min, [27]) and ^{213}Bi ($T_{1/2}$ = 45.61(6) min, [27]), respectively. Because of very short half-lives of ^{212,213}Po, often their α particles are measured with energies summed with

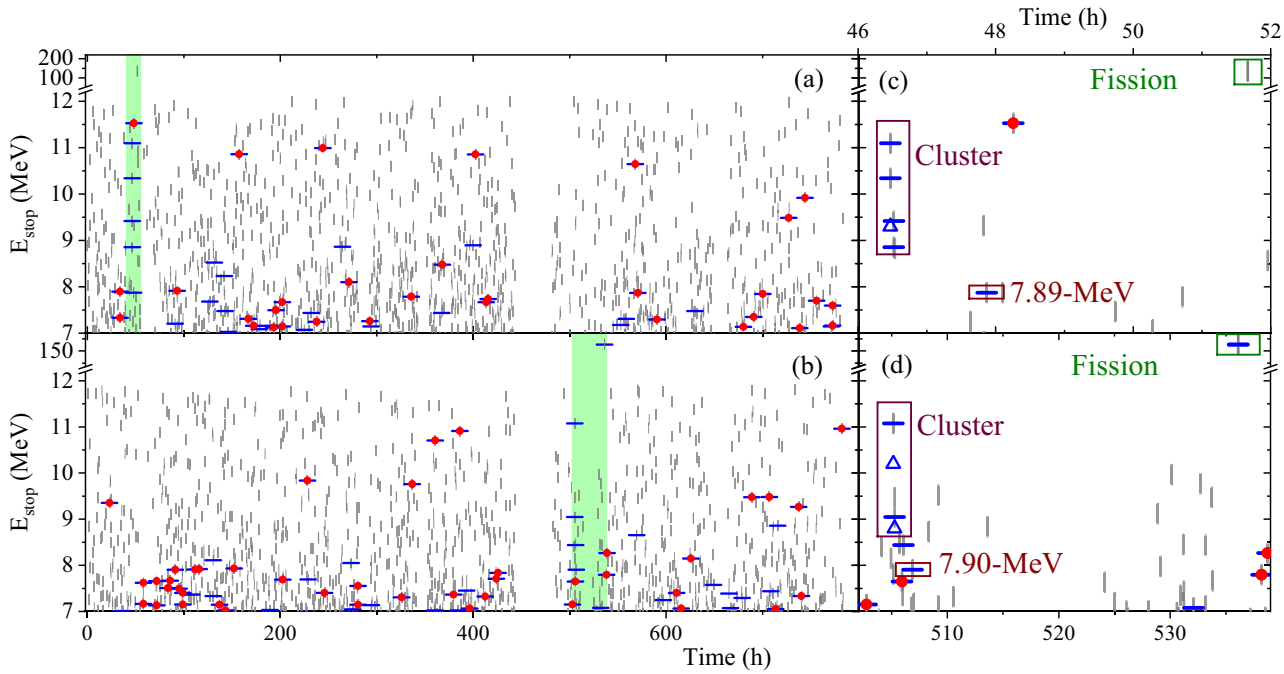

FIG. 5. Stop detector energies of anti-MWPC (vertical lines) and beam-off (horizontal lines) events in the pixels $X/Y = 103/41$ (a) and 111/19 (b) are shown as function of time, start from the beginning of the experiment. In the left panels, the time scale covering the entire experiment is shown. Shaded regions mark time windows where the chains #1 and #2 and fissions were detected. An expanded view of the time around these shaded regions is shown in the right panels (c,d). Identified beam-off α-like events with energies of 7–12 MeV are marked by squares. In the right panels, the α members of cluster-events reconstructed from stop and box detectors are shown by triangles. For details, see text.

electron energies. In the present experiment, such electron-α pile-up events could be resolved (see Appendix B).

Fifteen beam-off α-like events with energies of 7–8 MeV could not be unambiguously identified via the correlation analysis, but likely originate from long-lived (>1 s) nuclei produced in nonfusion reactions.

A small beam-off signal in between the third and fourth members (α_2 and α_3) was stored only in the digital branch, i.e., in the strip $Y = 41$ but without X-strip information. This beam-off event with a stop detector energy of 0.6 MeV was registered with a coincident signal in a box detector. Its total energy of 9.3(3) MeV was reconstructed. The counting rate for such events with reconstructed full energies of 8–10 MeV in strip $Y = 41$ with missing X signal was about 1.0×10^{-5} /s during beam-off periods, corresponding to an average appearance every 28 h. Taking into account the negligible random probability to observe this event exactly in between several beam-off α-like events occurring within 0.07 h ($\ll$ 28 h), this signal was attributed to be the fourth member of chain #1, registered 5.96 s after α_2. Taking this finding into account, a partial decay chain consisting of six nuclei with α-particle emission was established. Hereafter we will refer to these six α-like and ER events (see Table II) as a single cluster event. The random probability for observing chains similar to this cluster event is very low. By taking counting rates for ER-like and six α-like events within the ranges of 3–20 MeV and $E_\alpha \pm 1$ MeV, respectively, and measured correlation times, a probability of 2.4×10^{-21} was calculated for the random sequence of events like the chain #1 according to Ref. [48]. We note that this value could even be smaller if only nonidentified α-like events would be considered as a source for random correlations.

In between the cluster event and the fission event, four beam-off α-like events with energies of 6.82, 7.89, 11.53, and 6.29 MeV were detected (cf. Fig. 5 top right). Trace and event-by-event analyses proved the 11.53 MeV event to be a pile-up and a member of an ER-α(^{219}Ra)-α(^{215}Rn)-α(^{211}Po) sequence. The α-like event with 6.82 MeV was found to be correlated with an implantation signal with an energy of 32 MeV within 1.3 ms. However, no such α decay is known. Such short lifetimes typically correspond to higher α-particle energies, and accordingly we assume that in the present case, only part of the full energy was recorded. The 6.29-MeV event was followed by another beam-off α-like event detected 0.6 s later. It was attributed to the decay of the nonfusion product ^{220}Rn ($E_\alpha = 6.288$ MeV, [27]).

For the 7.89-MeV event no ER-like signal with any energy and in fact no event at all up to 135 s and 28 s, respectively, was detected. No subsequent α member of its potential chain was observed. If this high energetic (>7.6 MeV) α particle originated from a nonfusion product, then the preceding event (either an implantation signal or the α decay of the mother nucleus) would have to be detected within 1 s. Accordingly, it was not possible to attribute this event to originate from nonfusion products. Furthermore, this was the only event left without an attribution to nonfusion products from a total of ten events detected during the entire experiment within the energy range of 7.7–8.2 MeV in this pixel, where possible candidates

for members of the decay chain originating from ^{294}Ts have been discussed [23].

In pixel $X/Y = 111/19$, where chain #2 was found, 68 beam-off α-like events within $E_{\rm stop} = 7$–12 MeV were detected. 44 of them were found to be correlated to other members of their genetic relatives originating from the decay of nonfusion products. Seven beam-off α-like events with $E_{\rm stop} = 8$–12 MeV were not identified. Two of them belong to chain #2.

A signal with an energy of $E_{\rm stop} = 4.64$ MeV was detected during a beam-off period in between α_2 and α_3 of chain #2 and attributed to be a member of this chain. It was likely emitted into the backward direction under a rather shallow angle, thus leaving a relatively large fraction of its energy in the stop detector, but was not detected in the box detector. The counting rate of such beam-off events within the energy range of $E_{\rm stop} = 3$–6 MeV was about 4×10^{-5} /s which is similarly low as beam-off α-like events (cf. Table I). Therefore, this signal detected 2.35 s after the α_2 event was attributed to chain #2. With this additional member, the upper part of the chain #2, which has seven members detected within a short time window of 0.12 h becomes similar to the cluster event of chain #1. The random probability to observe the cluster event of chain #2 was estimated in the same approach as for chain #1 and is found to be on the order of 10^{-21}.

Nine beam-off α-like events with energies of 6.66, 7.65, 8.44, 7.90, 6.17, 6.72, 5.67, 7.08, and 6.61 MeV were detected in between the cluster and fission events of chain #2. The first two α particles were found to be associated with the α-decay chain of ^{220}Fr ($E_\alpha = 6.68$ MeV, [27]). No correlated members for the 8.44 MeV event were found. This event can be attributed to $\alpha(^{213}{\rm Po}) + \beta^-(^{213}{\rm Bi})$ pile-up as mentioned previously (see Appendix B).

No correlation members for the five low energetic (6.17, 6.72, 5.67, 7.08, and 6.61 MeV) α-like events were found, however, likely they originate from long-lived nuclei produced in nonfusion reactions. For the relatively high energy 7.9 MeV event, no ER-like and no event at all were detected within 113 and 33 s, respectively.

Finally, both decay chains contain a cluster event and a fission. Moreover, in both cases, beam-off α-like events with the same energy, 7.89(3) and 7.90(3) MeV, were observed in between the cluster and fission. Traces of these two α-like events contain a single signal in both cases, and no events back to 28 and 33 s were detected in the corresponding pixels. An origin of nonfusion products that emit the α particles with energies >7.6 MeV can easily be identified, because they have half-lives shorter than 0.4 s (cf. Appendix A 1). Ten and eleven α-like events with energies 7.7–8.2 MeV were detected in the pixels corresponding to chains #1 and #2, respectively. Only those two were left without an assignment to any of the nonfusion products. Therefore, a possible interpretation is that these two events might be associated with observed decay chains containing the cluster event and the fission each. The rate of α-like events within the wider energy range of 7.5–8.5 MeV still remains low; 15 and 22 events were detected in pixels 103/41 and 111/19 during the entire experiment, respectively, and only three and six of them remained unidentified.

The random probability to observe the cluster event is very small, thus for estimation of the random probability for observing various sequences of cluster–α(7.89-MeV), cluster–SF and cluster–α(7.89-MeV)–SF correlations we use the cluster-event as a 'single' event. The random probabilities to observe cluster-SF correlations were 3.1×10^{-2} and 6.0×10^{-2} for chains #1 and #2, respectively. Then, the random probabilities to find a sequence of cluster–α(7.5–8.5 MeV) are 4.0×10^{-2} and 6.9×10^{-2} for chains #1 and #2, which are similarly low as the values for cluster-SF correlations. These estimated random probabilities will further be reduced if only those three and six nonidentified beam-off α-like events are considered as a main source for random events. Finally, each triple sequence resulted in random probabilities of 8.6×10^{-4} and 2.2×10^{-3} for chains #1 and #2, respectively. Thus, these events are most probably genetically correlated. Moreover, decay properties of the corresponding members of both chains are compatible with one common origin. Therefore, based on the above mentioned analyses, two α-like events at 7.89(3) and 7.90(3) MeV were attributed to being members of the long-decay chains. Constructed full decay patterns are shown in Fig. 6, together with the traces of all members. All signals from α particles are recorded as single-signal traces. This allows to safely exclude pile-ups as source of any member of these two decay chains, as mentioned in the previous section.

Another interesting observation was the detection of a small additional signal in the trace of the ER from chain #1 (see Fig. 6). The energy of this signal was about 1.6 MeV and it follows the ER after 2.3 μs. The analysis of a variety of possible origins of this signal led to the conclusion that it was most probably of random origin, cf. Appendix B.

The first and second α particles having energies in excess of 10 MeV and short correlation times point towards the events having an origin from SHN. Isotopic assignment of these long decay chains can be made based on the properties of the odd-odd nuclei, which have an enhanced fission stability due to their unpaired proton and neutron. In such cases, members of the decay chains have an enhanced α-decay branching, and thus genetic correlations can be continued down to nuclei where α decay is not favorable anymore.

We compare these two long-decay chains to DGFRS data where four similarly long-decay chains have been reported and assigned to ^{294}Ts (cf. Fig. 6). Decay properties of members of the present two chains and DGFRS long chains are in agreement down to ^{270}Db. Therefore, the chains in this study were attributed to ^{294}Ts as well [12].

However, in all four ^{294}Ts chains from DGFRS, the end point of the chain was assigned to be ^{270}Db with a relatively long half-life. The measured correlation time to a preceding member (Δt) for the fission of ^{270}Db in the four chains of the DGFRS data were 33 h, 38 h, 24 h, and 1.2 h [21–23]. Only in the latter case, no α-like event in between the decay of ^{274}Bh and fission was observed in the beam shut-off period that continued until the detection of the fission event ([21–23]). In the other three chains, α-like events in the energy range of 7.7–8.2 MeV were detected. However, these events could

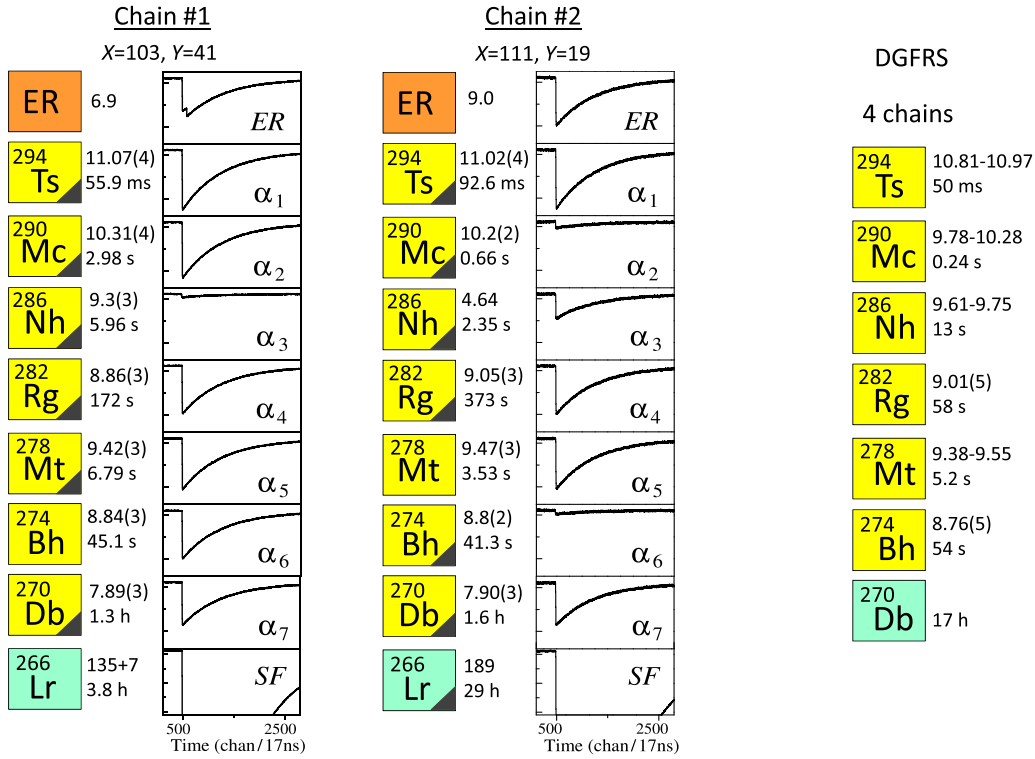

FIG. 6. Suggested decay sequence of the long α-decay chains observed during the 254 MeV-run (chain #1) and 258 MeV-run MeV (chain #2). Experimental energies in MeV and Δt are given for all events. Boxes with black triangles indicate events observed during beam-off periods. The measured fission-fragment energies are from stop+box detectors. Corresponding traces of all members of the chains are shown on the right side of the chains. A summary resulting from α-decay chains observed at DGFRS [23] is also shown.

not be assigned [21–23]. In the present experimental data the α-like event could be assigned to occur in between the decay of ^{274}Bh and fission of the long decay chains. Therefore, we suggest that ^{270}Db has an α-decay branching based on the observation of the 7.89(3) and 7.90(3) MeV α-like events. Thus, the decay sequence of ^{294}Ts was extended down to ^{266}Lr, which decays by fission. It is worth to note that a possible EC-decay branching of ^{266}Lr, which would likely result in the fission of ^{266}No, is expected to be small ($\lesssim$1%) according to systematics given in Ref. [21].

We note that theoretically predicted decay properties for members of the ^{294}Ts chain [49] are in good agreement and describe our findings down to ^{266}Lr [12,20].

For the DGFRS chain with the shorter Δt fission event, the chain is most likely terminated by fission of ^{270}Db. For the other three chains where fissions have considerably longer correlation times, the α decay of ^{270}Db may have been registered but could not be assigned (as considered in [21–23]) according to the present two chains.

The half-lives of ^{266}Lr and ^{270}Db derived from the present two fission events and from three events (one fission event from DGFRS and two α events from the present work) are 11^{+21}_{-5} h and $1.0^{+1.9}_{-0.4}$ h, respectively. If so, a branching ratio for fission of about $1/6 = 17\%$ is deduced for ^{270}Db. The partial fission half-lives for ^{266}Lr and ^{270}Db of 11^{+21}_{-5} h and $\approx$6 h fit well into the systematics of the partial spontaneous fission half-lives of known isotopes [45].

D. Short decay chains

Two shorter decay chains #3 and #4 consisting of six and four correlation members were observed at beam energies $E_{\rm lab} = 254.0$ and 258.0 MeV, respectively. These two chains occur within much shorter time periods compared to the long chains. The complete data on these chains are given in Table II. Traces of each member where only single signals were stored are shown in Fig. 7.

Both chains were detected with Y signals split into two neighboring strips except for the α_2 member of chain #3. Both shorter chains were detected in X strips located on the low magnetic rigidity side, where counting rates of nonusion products were high. Thus, the spectroscopic performance of these strips deteriorated over the course of the experiment, which increased the probability to register a split Y signal.

Detailed event-by-event analysis between the ER and SF members of chain #3 in the pixel $X = 47$ and $Y = 25/26$ showed that only one additional anti-MWPC event with an energy of 2.74 MeV was detected in between the third (α_2) and fifth (α_4) members of the chain (see Table II). Its split Y signal points to its belonging to chain #3. No box-signal was detected. This can be a hint that an α particle escaped into the open hemisphere of the FPDS.

Since the position of implantation of the heavy nucleus remains unchanged during its further decays because of a negligible recoiling effect of the α emission, subsequent signals detected from decays of daughter nuclei will also be

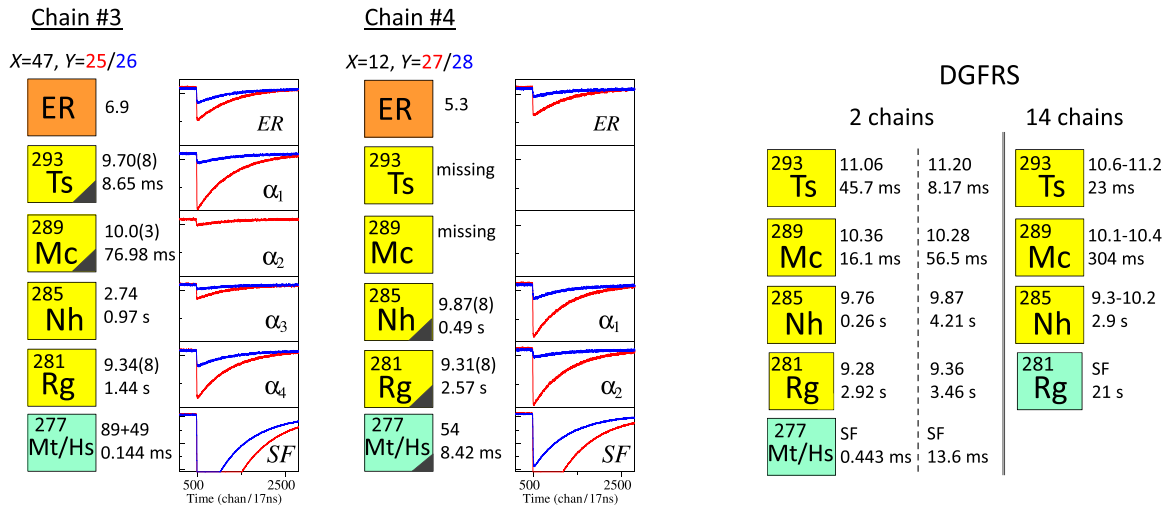

FIG. 7. Suggested decay sequence of two short α-decay chains observed during the 254 MeV-run (chain #3) and 258 MeV-run MeV (chain #4). Summaries of the 16 short decay chains observed at DGFRS and attributed to the decay of ^{293}Ts [20–23] are also shown for comparative discussion. Energies and correlation times of all individual members are given for two DGFRS chains that end by fission of either ^{277}Mt or ^{277}Hs. For each member of the "14 chains", an average half-life was calculated from those data, where the correlation time was measured relative to the mother nucleus. Isotopic assignments of chains #3 and #4 are made based on the DGFRS findings. In the case of chain #4 only one of several possible scenarios is given. Boxes with black triangles indicate events observed during beam-off periods. The measured fission fragment energies are from stop+box detectors. The corresponding traces of all members of the chains are shown on the right side of the chains. For more details, see text.

divided into two Y strips. The ratio between charge-sharing will roughly be conserved if the ER energy is split between two Y splits. As one can see in Fig. 7, the ratios of amplitudes (corresponding to energies) registered in $Y = 25$ and 26 are similar, and small variations are due to varying emission angles of the α particles. In case of the third (α_2) member, only one signal (in $Y = 25$) was detected. Because of the small energy (1.04 MeV) deposited in the stop detector by this escape α particle, the charge-sharing to the neighboring $Y = 26$ strip was not detectable. We note that in the pixel $X/Y = 47/25$ only 12 beam-off α-like events were detected within the energy range of 8.5–12.0 MeV during the entire experiment and five of them were pile-up events. Four of the remaining events were detected with a split Y signal. Similarly, two fissions were detected in the pixel $X/Y = 47/25$, only one of them had a split signal leaking into $Y = 26$. The random probability for chain #3 was estimated as 1.3×10^{-19} by taking counting rates of events within the range of $E_\alpha \pm 1$ MeV and without requiring Y split in $X/Y = 47/25$ pixel.

No additional event between ER and SF was found in the data for the second short chain #4. Traces of four members of this chain are also shown in Fig. 7. The ratio of the signal split between neighbours remained similar throughout the chain member events. The random probability for chain #4 was estimated as 8.5×10^{-12}. These probabilities were calculated without taking into account the Y split, which would result in even smaller values.

Similarly small energies (<10 MeV) of the first α-like events in both chains did not allow to attribute them right away to Ts or Mc [2,11,13,15,49]. Moreover, their correlation times to ER-like signals are quite different, indicating decays from different states and/or nuclei.

In the case of chain #3, the second α member has a relatively high energy that could be considered to be originate from decay of Ts-Nh [2,11,13,15,49]. Accordingly, it might be that the first α-decay energy in this chain #3 was not fully detected in the stop detector. Such a scenario can also be derived from the analysis of the correlation time of the 9.7 MeV α-like event according to well-known relations between the half-life and Q value of the α decay [49]. By considering 9.7 MeV as being the full energy of the α particle originating either from Ts, Mc, or Nh, one estimates half-lives of more than 1 s in all cases according to expressions given in Ref. [49]. These are significantly longer than the measured 8.65 ms correlation time. Therefore, likely, the 9.7 MeV is a partial energy of the α particle, which was emitted in a direction where part of its energy was not collected in the stop detector, similarly to the case of the 4.64 MeV event observed in chain #2.

In the case of chain #3, the first three α-decaying members show similar properties to the members of the long-decay chains, except for the energy of α_1. However, the properties of the fourth α and of the fission members significantly deviate from those in the two long chains (#1 and #2). Taking into account the odd-odd hindrance factor for spontaneous fission, it is unlikely that an isomeric state in ^{278}Mt can decay by fission directly. However, it could happen that the isomeric state decays into the daughter, even-even ^{278}Ds, which in turn rapidly fissions. Accordingly, based on the above assumptions one could attribute chain #3 as originating from ^{294}Ts and terminating by fission of ^{278}Ds produced in the electron capture decay of an isomeric state in ^{278}Mt. However, such an interpretation based on a single chain is highly speculative. Therefore, presently, our data can only be comparatively discussed relative to findings from the DGFRS,

where isotopic assignments for the observed short chains have been given [2,21–23].

Sixteen short-decay chains observed at DGFRS have been attributed to originate from the decay of ^{293}Ts formed in the 4*n* channel of the ^{48}Ca+^{249}Bk reaction. Most of these chains (14) were observed to terminate by fission at ^{281}Rg. Only in two cases were α decays of ^{281}Rg followed by short fission activities found. This short-lived fission activity could be originating from either ground or excited states in ^{277}Mt, or decay of ^{277}Hs produced as a daughter of ^{277}Mt decaying by EC as discussed in Ref. [23]. The decay properties of two chains are given in Fig. 7 together with compiled decay properties of the 14 shorter chains.

First, we note that despite a difference in the numbers of the members, nevertheless, the last two members in each of our chains (#3 and #4) are quite similar. Each chain ends with a fission with short correlation time (0.144 and 8.42 ms) following α particles with energies of 9.34(8) and 9.31(8) MeV, respectively (see Fig. 7). Based on this, we assume that the last two members of these chains likely originate from the same nucleus. Moreover, the last two members of our two short chains are similar to the last two members observed in two chains at DGFRS, where the sequence was attributed to ^{281}Rg–^{277}Mt/^{277}Hs. Moreover, chain #3 has the same number of members and their correlation times are in good agreement with data from DGFRS. Therefore, we conclude that chain #3 originates from the same nucleus as those two found at DGFRS. Thus, we attribute this chain to the decay-pattern of the chain assigned to ^{293}Ts from the DGFRS.

The discrepancies between chain #4 and that assigned to ^{293}Ts at DGFRS are obviously much more pronounced. Therefore, only a suggestive assignment relative to the DGFRS data can be given. One possible scenario is given in Fig. 7 where α particles from decays of ^{293}Ts and ^{289}Mc are scattered at open backward direction with small energy depositions in the stop detector, thus not generating signals above the ≈500 keV threshold. We note that the ER energy of this event is the lowest among our four chains. Accordingly, the implantation depth, which affects the energy release of backward scattered α particles, is smaller than in the case of the three other chains.

E. Cross sections

In the present work, one long and one short decay chain each were observed at two different beam energies $E_{\rm lab}$ = 254.0 MeV and 258.0 MeV. No chain was observed at a beam energy of $E_{\rm lab}$ = 252.1 MeV. Cross sections were deduced taking into account the decrease of ^{249}Bk target material as discussed earlier (see Fig. 1). Cross sections of the long decay chains attributed to the 3*n* channel of the ^{48}Ca+^{249}Bk fusion reaction are shown in Fig. 8 (upper panel) together with results from DGFRS [2]. Cross sections of the short chains are shown in Fig. 8 (lower panel) compared to those assigned to the formation of ^{293}Ts in the 4*n* channel.

Error bars and upper limits for cross sections were calculated according to Ref. [48]. The absolute values of cross sections obtained at TASCA and DGFRS are in agreement

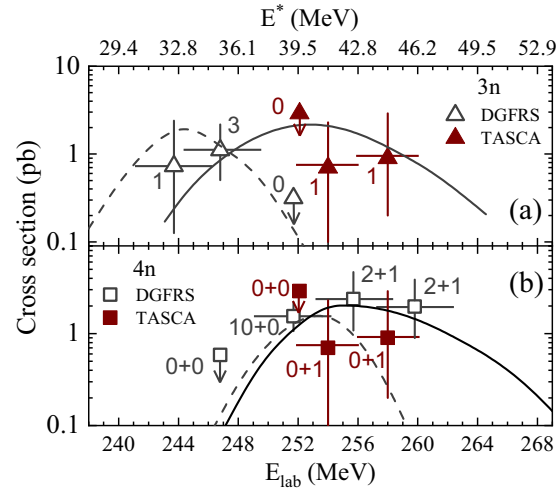

FIG. 8. Cross sections for the production of Ts nuclei in the ^{48}Ca+^{249}Bk reaction observed in the present work and from DGFRS [20,23]. (a) 3*n* channel from the fusion reactions where long-decay chains were assigned to ^{294}Ts. Numbers of observed chains are given. (b) Cross-section values corresponding to short-decay chains assigned to ^{293}Ts according to DGFRS are shown together with the sum of the observed number of chains terminating at ^{281}Rg and ^{277}Mt/^{277}Hs. Cross sections of the present chains ending with short-lived fission activity are also given. Solid and dashed lines mark the theoretically predicted cross section values adopted from Refs. [50] and [51], respectively. Excitation energies were calculated using the mass-table data from Refs. [32,33].

while the beam energies deviate. At DGFRS no simultaneous detection of both long and short decay chains at one particular beam energy (as was the case at TASCA) had been observed. In particular, the nonobservation of the long decay chains (associated with the 3*n* channel) at higher excitation energies was in contradiction to theoretical calculations from Ref. [50], which described most fusion-evaporation reactions of ^{48}Ca with actinide targets well. At the same time, the DGFRS results are well described by the calculations from Ref. [51], where significantly narrower excitation functions for both, the 3*n* and 4*n* channels were obtained (cf. Fig. 8).

In the present experiment, long-decay chains were observed also at beam energies higher than those used at DGFRS (cf. Fig. 8). We note that without taking into account the cross section limit from DGFRS at $E^* \approx 39$ MeV, the remaining data show a reasonable distribution for the excitation function of the 3*n* channel and agree with the calculations from Ref. [50].

In the DGFRS data, most of the statistics on chains assigned to the decay of the fusion products formed in the 4*n* evaporation channels have been collected at $E^* \approx 39$ MeV whereas no chains from the 3*n* channel were observed at that energy. The measured excitation function for the 4*n* channel at DGFRS agrees with the predictions from both Refs. [50,51].

Another interesting feature of the cross sections of the 4*n* channel from DGFRS can be seen. The cross sections of this channel have mostly been deduced from the set of 14 short decay chains terminating at ^{281}Rg (cf. Fig. 7). Ten

of those chains were detected at $E^* \approx 39$ MeV in two 70-d long experimental campaign at DGFRS (with one event being produced on average after beam doses of 4.8×10^{18} and 2.4×10^{18} particles in the first [20] and second [22] experiment, respectively) and the others at higher energies. In the present experiment, at $E^* \approx 39.2$ and 40.9 MeV, beam doses of 4.9×10^{18} and 2.3×10^{18} particles were accumulated [12], respectively. Taking into account the above production rates from DGFRS and the amounts of ^{249}Bk material in the targets, the nonobservation of short chains ending at ^{281}Rg in the present experiment can be attributed to the effect of rare-event statistics [48].

At DGFRS, two short chains ending with fission in ^{281}Rg and an additional one ending at ^{277}Mt/^{277}Hs have been measured at $E^* \approx 41$ and 44 MeV, respectively. These data give the α-decay branching of $1/3 \approx 33\%$ for ^{281}Rg. Based on this, one might expect the detection of up to five chains ending at ^{277}Mt/^{277}Hs in the DGFRS experiments at $E^* \approx 39$ MeV. This, though, was not the case [23]. Again, this could be due to rare-event statistics.

The present two short decay chains, suggestively attributed to terminate at ^{277}Mt/^{277}Hs, were observed at energies higher than $E^* \approx 39$ MeV similar to the results from DGFRS.

In summary, the beam energies corresponding to measured chains show some deviations between the present experiment and the results from DGFRS. In previous experiments on the production of Fl and Mc at TASCA, we did not observe significant deviations from DGFRS in the used beam energies. Taking into account the low statistics, we cannot draw any firm conclusions concerning deviations on the used beam energies, which may include systematic uncertainties in accelerator beam energies, target production, thickness estimation and the uniformity of the target surfaces between the experiments at TASCA and DGFRS.

IV. SUMMARY AND CONCLUSION

The fusion-evaporation reaction ^{48}Ca+^{249}Bk leading to the formation of the element Ts was successfully performed at the gas-filled recoil separator TASCA. A comprehensive analysis of the measured data obtained with a combined analog and digital data acquisition system was described in detail.

In total, four nonrandom α-decay chains were detected. Two of them were in agreement with each other and were attributed to the decay of ^{294}Ts. In both long chains an additional 7.89-MeV α particle was registered, compared to the chains from DGFRS, and was assigned to the decay of ^{270}Db. Combining the data from DGFRS and TASCA, a half-life of $1.0^{+1.9}_{-0.4}$ h was attributed to ^{270}Db, which suggestively has 83% and 17% branchings for α and fission decays, respectively. For ^{266}Lr, fission with a half-life of 11^{+21}_{-5} h was measured.

Another two chains were in less good agreement with each other. Their origin is suggested via a comparison with the reported decay patterns of ^{293}Ts from DGFRS.

Absolute cross section values measured for long and short decay chains were in agreement with values obtained at DGFRS. However, some deviations between the present and the DFGRS data can be noticed, especially for long-decay chains. They could be attributed to uncertainties associated with small numbers of observed events, target production, and accelerator beam energies. A continuation of the study of the ^{48}Ca+^{249}Bk reaction in the future with improved statistics and a dedicated measurement of the excitation functions of evaporation channels will help to make these findings more conclusive.

Finally, we conclude that our results from the investigation of the evaporation residues from the unique ^{48}Ca+^{249}Bk reaction confirm the synthesis of Ts isotopes, initially reported by DGFRS.

ACKNOWLEDGMENTS

We are grateful for GSI's ECR ion-source and UNILAC staff, and the Experimental Electronics department for their continuous support of the experiment. This work was financially supported in part by the German BMBF (05P12UMFNE), the Helmholtz association (VH-NG-723), the Australian Research Council, the Swedish Research Council (VR 2011-5253), the U.S. Department of Energy by LLNL (DE-AC52-07NA27344), the Laboratory Directed Research and Development Program at LLNL (11-ERD-011), and the Helmholtz Institute Mainz. This work was co-sponsored by the Office of Science, U.S. Department of Energy, and supported under U.S. DOE Grant No. DE-AC05-00OR22725. Three of us (J.M.G., K.E.G., H.N.) were supported by the U.S. Department of Energy, Office of Science, Nuclear Physics, Low Energy Physics Program, through the Lawrence Berkeley National Laboratory under Contract No. DE-AC02-05CH11231.

APPENDIX A: ANALYSIS OF THE EXPERIMENTAL DATA

1. Identifications of nonfusion products

Besides the implantation of ER from ^{48}Ca+^{249}Bk, significant amounts of nonfusion products have been implanted into the stop detector (cf. Fig. 3). Predominant amounts of these types of nuclei (which typically have smaller average magnetic rigidities than the set value) are strongly deflected by the dipole magnet and thus do not pass through TASCA. However, nuclei produced in nonfusion channels of the nuclear reaction can have kinematic properties that lead to a very broad magnetic rigidity distribution. Thus, a fraction evidently still can pass through TASCA and implant into the stop detector. As seen from Fig. 3, many α-like events and fissions were detected. Accordingly, prior to the main analysis to search for the decay of Ts, we identified the origins of detected α-like events. Such an analysis is very helpful for the identification of the rare radioactive decays of interest in the case when the background is high [52].

Possible candidates for implanted nuclei, which decay by α particle emissions with energies exceeding 7.6 MeV, are shown in Fig. 9 by their $T_{1/2}$ against α-particle energies. The figure includes cases with α-decay branches of $>10\%$ [27]. Two groups of nuclei can be seen in Fig. 9: those with $A < 240$ and those with $A \geqslant 240$. The half-lives of nuclei in the $200 \leqslant A < 240$ region are shorter than 0.4 s, except for

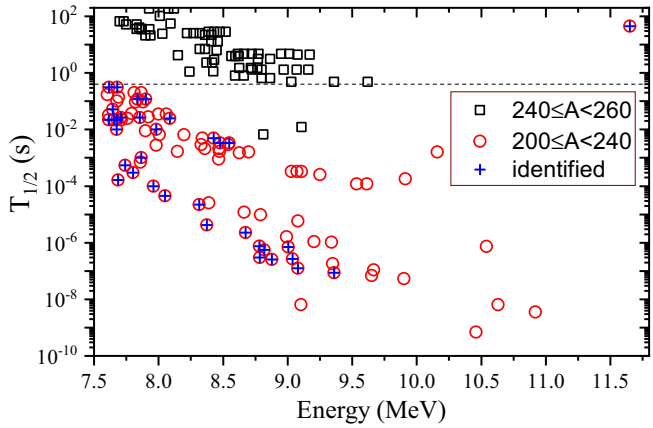

FIG. 9. Half-lives of potential candidates for two regions of nuclei with different atomic mass numbers ($200 \leqslant A < 240$ and $240 \leqslant A < 260$) produced in the ^{48}Ca+^{249}Bk/^{249}Cf reactions are shown by open symbols as function of their α-particle energies. Only those α-decay branches with absolute intensities and α-particle energies exceeding 10% and 7.6 MeV, respectively, are compiled. Isotopes identified in the analysis of the present data are marked by plus signs. A time level of 0.4 s at which most of the data can be separated into two groups is indicated by the dashed line.

^{212m}Po, while half-lives of the heavier ones (^{243}Es-^{260}Sg) are predominantly in excess of 1 s.

Different types of correlation analyses between implantation signal and/or α-like events were carried out. Implantation signals of nonfusion products typically have relatively high kinetic energies [53–55]. However, recently it was found that nonfusion products can also have relatively small kinetic energies [47]. Therefore, in the present analysis the implantation signals of non-fusion products were selected to be events in coincidence to an MWPC signal and within a wide energy range of 3–100 MeV.

As a result, α decays of $^{211–216}$Po, $^{212–217}$At, $^{213–220}$Rn, $^{214–221}$Fr, $^{219–222}$Ra, and $^{220–223}$Ac were identified. Those emitting α particles with energies exceeding 7.6 MeV are marked in Fig. 9. These nuclei are relatively short-lived and their identification via correlation analyses was straightforward, i.e., most α-like events were correlated with a first preceding event in the data. The energy distribution of these implantation signals shows a well pronounced single peak at around 40 MeV, with FWHM of ≈25 MeV. In turn, this explains the origin of events within an energy range of ≈(20–80) MeV in the high energy spectrum with coincident to MWPC signals (cf. Fig. 3). No low energy component as seen in the ^{50}Ti + ^{249}Cf reaction [47] was observed, which may indicate a different collision kinematics (e.g., used beam energies) and/or dynamics.

From the α decays of the above mentioned nuclei, different types of pile-up events, e.g., $\alpha(^{217}$Rn)–$\alpha(^{213}$Po) or $\alpha(^{216}$Rn)–$\alpha(^{212}$Po) were generated in the stop detector and were identified thanks to CANDI. These pile-ups occurring in a wide range of energies as shown in Fig. 3 are one of the main sources for candidates of decays originating from SHN. Overall, every single uncorrelated α-like event with an energy of >7.6 MeV was attributed to belong to the decay of a nonfusion product, if it was preceded by a stop-detector signal within 1 s.

TABLE III. Examples of random chains observed in ER–α–α, α–α–α, and ER–α–α–SF analyses. Energies and correlation times relative to preceding members are given. Bold font values indicate beam-off events. Details are given in the text.

Chain #	*a*	*b*	*c*	*d*	*e*
Strips (X/Y)	23/26	54/41	4/46	6/27	31/30
			E (MeV)		
			Δt (s)		
ER	20.0	8.3	12.4		7.0
α_1	9.32	**11.24**[b]	**9.71**	8.83	10.77
	0.979	*0.00329*	*0.144*	–	*8.4*
α_2	8.90	9.50	**9.5**[a,b]	**10.82**[b]	9.03
	11.2	*8.70*	*7.27*	*12.0*	*37.3*
α_3/SF				9.0[a]	**97**
				137	*296.8*

[a]Total energy of event with coincident stop and box signals.
[b]Traces of these α-like events have multi signals, and are thus assigned as pile-ups.

In our experiment, about 13000 fission-like events were detected during the entire run. 60% of these were distributed in the left side of the DSSD ($X < 34$) similar to the case of α particles originating from nonfusion reactions (cf. Sec. III A). Only four fission events were identified to be correlated with α-decay chains and all remaining events were attributed to originate from transfer reactions around the ^{249}Bk target nucleus. Potential candidates for the origin of such fission events have been discussed in Ref. [55].

2. Analysis of candidates for nonrandom chains

a. Results of ER–α–α correlations

In the main analysis searching for the α-decay chains originating from Ts, for which search conditions are given in Sec. III B, about 1000 ER–α_1–α_2 correlations were found. Most of them contain two α-like events, both occurring during beam-on periods. One such chain (labelled as #*a*) is shown in Table III as an example. Characteristics, i.e., correlation times and energies of every member of this chain, are very close to the upper and lower limits of the correlation windows, respectively. These are in contradiction to the expected decay properties of SHN, whose α particles have higher energies and shorter correlation times according to known data [1,2,27] and theoretical predictions [49]. Furthermore, no other α- or fission-like events were found to be genetically correlated to the chain #*a*. Accordingly, this is an example for randomly correlated events where two beam-on α-like events are the main source for the random sequence. The distribution of these randomly correlated chains along the x axis is shown in Fig. 10(a). Their abundance increases towards the low magnetic rigidity side of the stop detector, where the counting rates were high.

125 and 11 chains with one and two beam-off α-like events, respectively, were found and their X distributions are shown

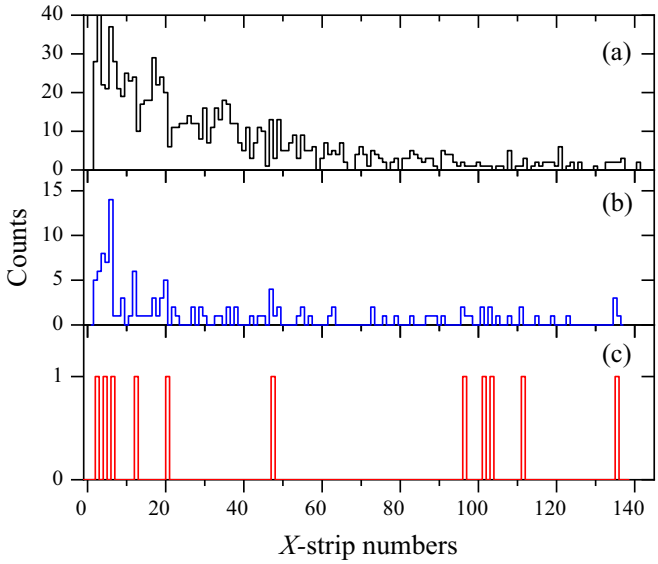

FIG. 10. Horizontal (X-strip) distributions of ER–α_1–α_2 chains containing (a) two beam-on α-like, (b) one and (c) two beam-off α-like events.

in Figs. 10(b)–10(c). Most of the chains with one beam-off α-like event are found to be random correlations. One such chain (#*b*), where the first α decay with 11.24 MeV occurred during a beam-off period, is also given in Table III. Inspection of the digital traces showed that the 11.24 MeV event is the pile-up, where two signals were detected within 2.5 μs. In a further detailed analysis, true genetically correlated members of the 11.24 MeV event which originates from the decay of ^{221}Ra, accordingly different from those found in chain #*b*, were found. Therefore, chain #*b* was attributed to be random.

The expected average number of random chains consisting of an ER-like and two beam-off α-like events was calculated as $\approx 5.8\times10^{-5}$ per pixel based on average counting rates given in Table I and by taking into account the beam structure. In total 11 such chains were observed and were inspected in detail event-by-event. Only four of them were found to contain traces measured only with a single signal. These were the chains discussed in connection with α decays from Ts in Secs. III C and III D.

The remaining seven chains were found to contain at least one pile-up beam-off signal. One of them is presented in Table III (labeled as chain #*c*) as an example. The α_2 member of this chain is a pile-up. In the event-by-event analysis, these two beam-off α_1 and pile-up α_2 events were found to be correlated with their true members (e.g., with high energetic implantation signals) of the different decay chains originating from ^{220}Ra and ^{220}Ac, respectively. Therefore, the correlation ER–α_1–α_2 sequence with these two beam-off α-like events (see Table III) is of random origin. The other six chains detected with two beam-off α-like events were assigned also to random origin on the basis of the results from the event-by-event analysis, which was similar to the case of chain #*c*.

b. Results of α–α–α and ER–α–α–SF correlations

Only three of 2000 chains with triple α-like events were identified as being nonrandom. They belong to members of chains #1 and #2 (α_3–α_4–α_5), and to chain #3 (α_1–α_2–α_3) (see Table II). One of the triple α chains observed with one beam-off α-like event is given in Table III (#*d*) and is representative also for the remaining random chains. In the event-by-event analysis, the origin of the beam-off α_2 member of the chain #*d* showed a two-signal trace and was found to be the pile-up, $\alpha(^{218}\text{Fr})$–$\alpha(^{214}\text{At})$, member of a decay chain originating from ^{222}Ac.

One of the 60 chains observed with ER–α_1–α_2–SF sequence is shown in Table III (#*e*), as a representative of most of the chains detected with two beam-on α-like events. Four chains containing at least one beam-off α-like event were found. Three chains were belonging to various combinations of the members of chain #3, i.e., ER–α_1–α_2–SF, ER–α_1–α_3–SF, and ER–α_2–α_3–SF (see Table II). The fourth ER–α_1–α_2–SF sequence corresponds to chain #4 (see Table II). All chains containing two beam-on α-like members were further inspected for the presence of additional members that occurred during the beam-off periods in between ER and SF, but no such event was found. Additionally, the decay properties of such chains (cf. Table III, #*e*) did not show any indication for originating from SHN [1,2,49], thus they were attributed to random correlations.

APPENDIX B: ORIGIN OF THE DOUBLE-SIGNAL ER TRACE IN CHAIN #1

The detected small-energy signal in the trace of the event like in the case of the ER from chain #1 [see Fig. 11(a)] can originate from different sources. It could be associated with a backward-scattered α particle, which leaves the stop detector with a small energy release. A typical signal registered as a backward-scattered α within a short time after implantation (ER) is shown in Fig. 11(b). In this case, the α particle of ^{219}Th (E_α = 9.34 MeV, [27]) was emitted 2.1 μs after the ER implantation into the stop detector with 15 MeV energy, in backward direction, imparting an energy of about 1.1 MeV. Then, the backward scattered α particle was detected in the box detector from which the residual energy of about 8.2 MeV was extracted.

If the 1.6 MeV signal detected shortly after the ER(^{294}Ts) is an escaping α particle, the box detectors register the additional signal ($\sim$ rest energy) with relatively high geometric efficiency. However, no such box detector signal was detected. From a geometric consideration, this would point to an emission into the open hemisphere of the FPDS. However, the nonobservation of such a signal in the ER of the second chain points to this small-energy signal as not being due to the detection of such an escape α particle.

Another possibility for the origin of this signal is the detection of electron(s) originating from β^- decay and/or internal conversion. In such cases, the nondetection of a small signal in the second chain is probable because of a low ionization efficiency. In Figs. 11(c) and 11(d), two cases where electrons were measured within a short time relative to the main signals are shown. The first case is the well-known

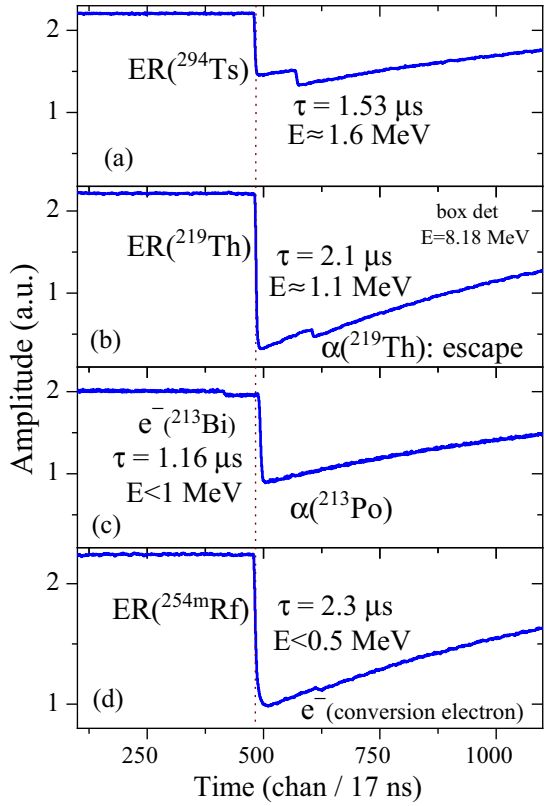

FIG. 11. Traces of various signals detected with small energetic signals. The origins of the triggering signals are given together with the energies for the smaller ones. Time differences between two signals are also given. For details, see the text.

decay of the relatively long-lived ^{213}Bi, which is often implanted during experiments on the synthesis of SHN as a nonfusion product [20]. Because of the short half-life of ^{213}Po ($T_{1/2} = 2.4$ μs, [27]), its α particle with an energy of $E_\alpha = 8.376$ MeV ([27]) is often registered with an additional energy associated with the detection of the electron from the preceding β^- decay of ^{213}Bi in standard conventional analog electronics [20]. As shown in Fig. 11(c), CANDI is well suited for resolving such cases; the energy of the electron was estimated to be less than 1 MeV in the present case where the α decay of ^{213}Po is the main triggering signal for data being collected. The preceding electron was detected prior to the main signal. Detection of electrons from the internal conversion originating from the de-excitation of the K-isomeric state in ^{254}Rf* [45] is also possible with CANDI, see Fig. 11(d). The measured energy of the shown example was estimated to be less than 0.5 MeV. In conclusion, by considering the detection efficiency of electrons with various energies in 300 μm Si, an energy of 1.6 MeV, as registered in the trace of the ER in chain #2 appears too high for originating from electrons. Thus, such scenarios are unlikely.

Finally, the most probable reason for observing such a signal is a random coincidence. As seen from Fig. 3, an event from the intense peak at around 1.5 MeV appears to be the most likely source for this small signal. The probability to observe such a signal associated with detection of light particles (e.g., proton) in the ER trace was estimated as <5% based on the measured α decay of ^{211}Po during the beam-on periods. While this is a relatively low value for randomly observing an ER(^{294}Ts) with such a signal, this seems to be the most likely reason.

[1] S. Hofmann and G. Münzenberg, Rev. Mod. Phys. **72**, 733 (2000).
[2] Yu. Ts. Oganessian and V. K. Utyonkov, Rep. Prog. Phys. **78**, 036301 (2015).
[3] K. Morita *et al.*, J. Phys. Soc. Jap. **81**, 103201 (2012).
[4] P. Armbruster *et al.*, Phys. Rev. Lett. **54**, 406 (1985).
[5] S. Hofmann *et al.*, Eur. Phys. J. A **32**, 251 (2007).
[6] L. Stavsetra, K. E. Gregorich, J. Dvorak, P. A. Ellison, I. Dragojevic, M. A. Garcia, and H. Nitsche, Phys. Rev. Lett. **103**, 132502 (2009).
[7] Ch. E. Düllmann *et al.*, Phys. Rev. Lett. **104**, 252701 (2010).
[8] P. A. Ellison *et al.*, Phys. Rev. Lett. **105**, 182701 (2010).
[9] J. M. Gates *et al.*, Phys. Rev. C **83**, 054618 (2011).
[10] S. Hofmann *et al.*, Eur. Phys. J. A **48**, 62 (2012).
[11] D. Rudolph *et al.*, Phys. Rev. Lett. **111**, 112502 (2013).
[12] J. Khuyagbaatar *et al.*, Phys. Rev. Lett. **112**, 172501 (2014).
[13] U. Forsberg *et al.*, Nucl. Phys. A **953**, 117 (2016).
[14] D. Kaji *et al.*, J. Phys. Soc. Jpn. **86**, 034201 (2017).
[15] J. M. Gates *et al.*, Phys. Rev. Lett. **121**, 222501 (2018).
[16] A. Türler, R. Eichler, and A. Yakushev, Nucl. Phys. A **944**, 640 (2015).
[17] J. Khuyagbaatar, EPJ Web Conf. **163**, 00030 (2017).
[18] J. Khuyagbaatar, EPJ Web Conf. **163**, 00068 (2017).
[19] J. M. Gates *et al.*, Phys. Rev. C **92**, 021301(R) (2015).
[20] Yu. Ts. Oganessian *et al.*, Phys. Rev. Lett. **104**, 142502 (2010).
[21] Yu. Ts. Oganessian *et al.*, Phys. Rev. C **83**, 054315 (2011).
[22] Yu. Ts. Oganessian *et al.*, Phys. Rev. Lett. **109**, 162501 (2012).
[23] Yu. Ts. Oganessian *et al.*, Phys. Rev. C **87**, 054621 (2013).
[24] J. Roberto *et al.*, Nucl. Phys. A **944**, 99 (2015).
[25] J. Runke *et al.*, J. Rad. Nucl. Chem. **299**, 1081 (2014).
[26] J. Chen, I. Ahmad, J. P. Greene, and F. G. Kondev, Phys. Rev. C **90**, 044302 (2014).
[27] http://www.nndc.bnl.gov/ensdf/.
[28] J. Khuyagbaatar *et al.*, GSI Scientific Report No. 2012 (2013), p. 131.
[29] E. Jäger *et al.*, J. Rad. Nucl. Chem. **299**, 1073 (2014).
[30] A. Yakushev *et al.* (unpublished).
[31] J. F. Ziegler, Nucl. Instrum. Methods Phys. Res. B **219**, 1027 (2004).
[32] G. Audi, A. Wapstra, and C. Thibault, Nucl. Phys. A **729**, 337 (2003).
[33] W. Myers and W. Swiatecki, Nucl. Phys. A **601**, 141 (1996).
[34] P. Möller *et al.*, At. Data Nucl. Data Tables **59**, 185 (1995).
[35] A. Semchenkov *et al.*, Nucl. Instrum. Methods Phys. Res. B **266**, 4153 (2008).
[36] A. Yakushev *et al.*, Inorg. Chem. **53**, 1624 (2014).
[37] J. Khuyagbaatar *et al.*, Nucl. Instrum. Methods Phys. Res. A **689**, 40 (2012).
[38] K. Gregorich, Nucl. Instrum. Methods Phys. Res. A **711**, 47 (2013).

[39] J. Khuyagbaatar, V. P. Shevelko, A. Borschevsky, C. E. Dullmann, I. Y. Tolstikhina, and A. Yakushev, Phys. Rev. A **88**, 042703 (2013).
[40] A. Gorshkov, A new focal plane detector for the gas-filled separator TASCA, Ph.D. thesis, Technical University of Munich (2010).
[41] I. Wegrzecka *et al.*, Proc. SPIE **8902** (2013).
[42] N. Kurz *et al.*, GSI Scientific Report No. 2011, (2012), p. 252.
[43] J. Khuyagbaatar *et al.*, GSI Scientific Report No. 2012, (2013), p. 133.
[44] J. Khuyagbaatar *et al.*, Phys. Rev. Lett. **115**, 242502 (2015).
[45] J. Khuyagbaatar *et al.*, EPJ Web Conf. **131**, 03003 (2016).
[46] A. Såmark-Roth *et al.*, Phys. Rev. C **98**, 044307 (2018).
[47] A. Di Nitto *et al.*, Phys. Lett. B **784**, 199 (2018).
[48] K. H. Schmidt *et al.*, Z. Phys. A **316**, 19 (1984).
[49] A. Sobiczewski, Acta Phys. Pol. **41**, 157 (2010).
[50] V. Zagrebaev and W. Greiner, Phys. Rev. C **78**, 034610 (2008).
[51] K. Siwek-Wilczyńska, T. Cap, M. Kowal, A. Sobiczewski, and J. Wilczynski, Phys. Rev. C **86**, 014611 (2012).
[52] J. Konki *et al.*, Phys. Lett. B **764**, 265 (2017).
[53] V. V. Volkov, in *Classical and Quantum Mechanical Aspects of Heavy Ion Collisions*, edited by H. L. Harney, P. Braun-Munzinger, and C. K. Gelbke, Lecture Notes in Physics Vol. 33 (Springer, Berlin, Heidelberg, 1975).
[54] S. Heinz *et al.*, J. Phys. Conf. Ser. **282**, 012007 (2011).
[55] S. Heinz *et al.*, Eur. Phys. J. A **48**, 32 (2012).